JGR Biogeosciences

RESEARCH ARTICLE
10.1029/2020JG006136

Key Points:

- Latitudinal differences in correlation between TROPOspheric Monitoring Instrument chlorophyll fluorescence and non-adjusted and bidirectional-adjusted vegetation indices
- Choice of solar radiance data product likely to yield substantial regional differences in estimates of the amount of sunlight absorbed by chlorophyll
- Modeling gross primary production as a non-linear response to photosynthetically active radiation would likely improve satellite-based estimates of gross primary production

Supporting Information:

Supporting Information may be found in the online version of this article.

Correspondence to:

X. Xiao,
xiangming.xiao@ou.edu

Citation:

Doughty, R., Xiao, X., Köhler, P., Frankenberg, C., Qin, Y., Wu, X., et al. (2021). Global-scale consistency of spaceborne vegetation indices, chlorophyll fluorescence, and photosynthesis. *Journal of Geophysical Research: Biogeosciences*, *126*, e2020JG006136. https://doi.org/10.1029/2020JG006136

Received 28 OCT 2020
Accepted 2 JUN 2021

Global-Scale Consistency of Spaceborne Vegetation Indices, Chlorophyll Fluorescence, and Photosynthesis

Russell Doughty[1,2], Xiangming Xiao[1], Philipp Köhler[2], Christian Frankenberg[2,3], Yuanwei Qin[1], Xiaocui Wu[1], Shuang Ma[3], and Berrien Moore III[4]

[1]Department of Microbiology and Plant Biology, University of Oklahoma, Norman, OK, USA, [2]Division of Geological and Planetary Sciences, California Institute of Technology, Pasadena, CA, USA, [3]Jet Propulsion Laboratory, California Institute of Technology, Pasadena, CA, USA, [4]College of Atmospheric and Geographic Sciences, University of Oklahoma, Norman, OK, USA

Abstract The new TROPOspheric Monitoring Instrument (TROPOMI) solar-induced chlorophyll fluorescence (SIF) data provides new opportunities to corroborate and improve global photosynthesis estimates. Here we report the spatiotemporal consistency between TROPOMI SIF and vegetation indices from the bidirectional reflectance distribution function (BRDF) adjusted (MCD43) and standard MODIS (MOD09) surface reflectance products, estimates of absorbed photosynthetically active radiation by chlorophyll ($APAR_{chl}$) derived from National Centers for Environmental Prediction Reanalysis-2 (NCEP2), MODIS MCD18, and European Reanalysis (ERA5) data, and two GPP products (GPP_{VPM} and GPP_{MOD17}). We find (a) non-adjusted VIs were more highly correlated with SIF at mid and high latitude than BRDF-adjusted VIs, but were less correlated in the tropics, (b) negligible differences in the correlation between SIF and non-adjusted NIRv and EVI, but BRDF-adjusted NIRv had higher correlations with SIF at mid to high latitude than BRDF-adjusted EVI but lower correlations in the tropics, (c) choice of PAR data set likely to cause substantial differences in global and regional GPP estimates and the correlation between modeled GPP and SIF, (d) SIF was more highly correlated with $APAR_{chl}$ at high to mid latitude than EVI but more highly correlated with EVI at lower latitudes, and (e) GPP_{VPM} is more highly correlated with SIF than GPP_{MOD17}, except in sub-Sahara Africa. Our results highlight that spaceborne photosynthesis would likely be improved by using a non-linear response to PAR and that the fundamental differences between the vegetation indices and PAR data sets are likely to yield important differences in global and regional estimates of photosynthesis.

Plain Language Summary The validation of global, satellite-based estimates of terrestrial photosynthesis has traditionally been conducted using a network consisting of a couple of hundred observation towers. However, these towers are not uniformly distributed across Earth's biomes and are largely concentrated in North America, Europe, and East Asia. Recent advancements in the detection of solar-induced chlorophyll fluorescence (SIF), which is emitted from plants during photosynthesis, from space now affords us an opportunity to further validate satellite-based photosynthesis and investigate how such estimates may be improved. The recently launched TROPOspheric Monitoring Instrument (TROPOMI) provides daily global scans at a relatively high spatial resolution. Here, we compare at the global-scale TROPOMI SIF to satellite-based photosynthesis, vegetation indices, and estimates of the amount of sunlight absorbed by chlorophyll ($APAR_{chl}$), the latter two of which are used for estimating photosynthesis. Although we found TROPOMI SIF to be consistent with satellite-based photosynthesis, vegetation indices, and $APAR_{chl}$, we found that SIF was better correlated with $APAR_{chl}$ at high to mid latitude and better correlated with EVI at lower latitudes. This discrepancy indicates that modeling GPP as a non-linear response to PAR would improve spaceborne estimates of photosynthesis.

1. Introduction

Global estimates of gross primary production (GPP) from various data-driven models and process-based models have traditionally been validated using the FLUXNET 2015 data set (https://fluxnet.fluxdata.org/), a global network of about 500 eddy flux towers (Pastorello et al., 2020). However, this network is largely concentrated in North America, Europe, and East Asia, which prevents the validation of GPP estimates

in many parts of the world. Recent scientific advancements enable us to retrieve solar-induced chlorophyll fluorescence (SIF) from spaceborne spectroscopic measurements (Frankenberg et al., 2011; Guanter et al., 2007; Joiner, Yoshida, Vasilkov, & Middleton, 2011), which is light energy emitted by plants after chlorophyll absorbs sunlight. Spaceborne SIF data has been shown to be linearly correlated with GPP at coarse spatial and temporal scales (Lin et al., 2019; Magney, Barnes, & Yang, 2020; Magney, Bowling, et al., 2019; X. Yang et al., 2015). Thus, spaceborne SIF has become an accepted proxy and is a new tool for assessing the performance of GPP products (Sun et al., 2017; Wagle, Zhang, Jin, & Xiao, 2016; Y. Zhang et al., 2016).

Photosynthesis begins with the absorption of photosynthetically active radiation (PAR) by chlorophyll in the leaves of a canopy ($APAR_{chl}$, $APAR_{leaf}$, and $APAR_{canopy}$). Over the past few decades, many vegetation indices (VIs) have been calculated using the blue, red, and/or near-infrared spectral bands of light reflected by Earth's surface as observed by satellite optical sensors. The Normalized Difference Vegetation Index (NDVI) (Rouse, Haas, Schell, & Deering, 1974) and Enhanced Vegetation Index (EVI) (Huete, Liu, Batchily, & van Leeuwen, 1997) have been respectively used to estimate the fraction of PAR absorbed by the canopy ($fPAR_{canopy}$) (Running et al., 2004) and by chlorophyll ($fPAR_{chl}$) (Xiao et al., 2004). $fPAR_{canopy}$ is substantially larger than $fPAR_{chl}$ because the canopy is composed of both chlorophyll and non-photosynthetic vegetation (Q. Zhang et al., 2005). $fPAR_{canopy}$ and $fPAR_{chl}$ are used to estimate $APAR_{canopy}$ and $APAR_{chl}$ (Equations 1 and 2).

$$APAR_{canopy} = fPAR_{canopy} \times PAR \tag{1}$$

$$APAR_{chl} = fPAR_{chl} \times PAR \tag{2}$$

$APAR_{chl}$ has three pathways: non-photochemical quenching (or heat; NPQ), photochemical quenching (chemical energy used for converting CO_2 to carbohydrate; PQ), and SIF (Equation 3).

$$APAR_{chl} = NPQ + PQ + SIF \tag{3}$$

Light use efficiency (LUE) models estimate the daily GPP (g C/m^2/day) of vegetation using $APAR_{canopy}$ or $APAR_{chl}$ and light use efficiency (ε_g), or the efficiency of plants to convert light energy into carbohydrates, using Equations 4 and 5:

$$GPP = APAR_{canopy} \times \varepsilon_g \tag{4}$$

$$GPP = APAR_{chl} \times \varepsilon_g \tag{5}$$

Two commonly used GPP data products from the LUE models include GPP_{MOD17} (MOD17) from the Moderate Resolution Imaging Spectroradiometer (MODIS) (Running & Zhao, 2015), which uses $fPAR_{canopy}$ and $APAR_{canopy}$, and GPP_{VPM} from the Vegetation Photosynthesis Model (VPM) (Xiao et al., 2004; Y. Zhang et al., 2017), which uses $fPAR_{chl}$ and $APAR_{chl}$.

The newly launched TROPOspheric Monitoring Instrument (TROPOMI) onboard the Sentinel-5 Precursor satellite provides SIF data with near-daily global coverage at much finer spatial resolutions (3.5 × 7 km at nadir) than previous platforms (Köhler et al., 2018). The new TROPOMI SIF data have provided valuable contributions to the debates over the seasonality of vegetation photosynthesis at regional scale, which has important implications for understanding the inter- and intra-annual variability of Earth's atmospheric carbon dioxide concentration (Doughty et al., 2019; Turner et al., 2019; Yin et al., 2020). To date, no study has conducted a global-scale correlative analysis of TROPOMI SIF data with vegetation indices (proxies for estimating $fPAR_{chl}$ and $fPAR_{canopy}$), $APAR_{chl}$ and $APAR_{canopy}$, and GPP estimates from data-driven models (e.g., GPP_{MOD17} and GPP_{VPM}). Here, we conducted these correlative analyses to answer five primary questions, which were aimed to provide insight into the relationships between SIF and $fPAR_{canopy}$, $fPAR_{chl}$, $APAR_{canopy}$, $APAR_{chl}$, GPP_{VPM}, and GPP_{MOD17}.

First, are bidirectional reflectance distribution function (BRDF) adjusted VIs more strongly correlated with SIF than non-adjusted VIs? BRDF adjustments to the MODIS surface reflectance data has been performed because of the sensor's sequential angular views over time can introduce slight artifacts or drifts in the data

(Morton et al., 2014; C. B. Schaaf et al., 2002). Thus, it has been argued that BRDF-adjusted VIs should be used when quantifying the changes of vegetation or estimating GPP, especially in the tropics, because the adjustment can help account for differences in viewing and illumination geometry between satellite observations (Morton et al., 2014). Others have pointed out that BRDF adjustment can have disadvantages (Huete et al., 2002) and that a BRDF adjustment marginally decreases the magnitude of the seasonal change in vegetation indices but does not change the seasonality itself (Guan et al., 2015; Maeda, Heiskanen, Aragão, & Rinne, 2014; Saleska et al., 2016). Similarly, it is known that sun-sensor geometry can impact retrieved SIF values, with higher SIF values at lower phase angles when the satellite sensor and the sun are nearly aligned (Joiner et al., 2020; Köhler et al., 2018). Here, we compared vegetation indices derived from both the non-adjusted MODIS standard surface reflectance (MOD09) and BRDF-adjusted surface reflectance (MCD43) products with SIF. We suspected that BRDF-adjusted NIRv and EVI would have a better relationship with SIF than non-adjusted VIs, because (a) the directionality of the escape of emitted SIF from the canopy has been suspected to be similar to the escape of reflected energy (P. Yang & van der Tol, 2018) and (b) we partially account for the effects of illumination and viewing geometry on retrieved SIF values.

Second, does the near-infrared reflectance (NIR) of terrestrial vegetation (NIRv have a higher correlation with TROPOMI SIF than EVI or NDVI? Recently, a study found that NIRv, the product of NDVI and the near-infrared band, had a stronger correlation with modeled GPP (FluxCom) than SIF (GOME-2) and suggested that NIRv could be a superior index when used to model global GPP (Badgley, Field, & Berry, 2017). A more recent study of 10 sites across several biomes found a near perfect correlation ($R^2 = 0.99$) between NIRv and EVI (Hinojo-Hinojo & Goulden, 2020). We expected a weaker correlation between SIF and NDVI than between SIF and EVI or NIRv because of NDVI's tendency to saturate in regions with a high leaf area index. More importantly, we expected to determine if there is a clear difference in the ability of EVI or NIRv to track changes in the vegetation canopy.

Third, how would the input of PAR data from the National Centers for Environmental Prediction Reanalysis-2 (NCEP2), the European Reanalysis (ERA5), and MODIS MCD18 affect the correlation between $APAR_{chl}$ and SIF? The NCEP2 data has a 6-h temporal resolution and a coarse spatial resolution of roughly 1.9° (T62 Gaussian grid). The other two data sets have higher spatial and temporal resolutions and were very recently published: the ERA5 product at 1-hourly and 0.10° and the MCD18 product at 3-hourly and 0.05°. Here, we compared their differences out-of-the-box, computed $APAR_{chl}$ from each data set, and compared $APAR_{chl}$ with SIF.

Fourth, does SIF have a higher correlation with $APAR_{chl}$ than VIs? We expected SIF to be better correlated with $APAR_{chl}$ than VIs, which are proxies of fPAR, because SIF is driven by both fPAR and PAR and thus has a strong empirical relationship with $APAR_{chl}$ at the leaf and canopy scales (Magney, Frankenberg, et al., 2019; Miao et al., 2018).

Finally, does GPP_{VPM}, an $APAR_{chl}$-based model, have a stronger spatial and temporal correlation with TROPOMI SIF than does GPP_{MOD17}, an $APAR_{canopy}$-based model? We expected GPP_{VPM} to be better correlated with TROPOMI SIF because VPM uses $fPAR_{chl}$ and SIF energy emitted by chlorophyll after it absorbs PAR.

2. Materials and Methods

Figure 1 illustrates a workflow and the data sets used in our study. All medians presented in the inset maps in the Results section below are presented together in Table S1.

2.1. TROPOMI SIF Retrievals

The retrieval of SIF from spaceborne sensors requires a moderate to high spectral resolution spectrometer to detect the changes in the optical depths of Fraunhofer lines caused by the weak fluorescence emission, which has been satisfied by spaceborne platforms that target trace gases in the atmosphere. The first retrievals of SIF from spaceborne platforms were described in a series of papers starting in 2007 (Guanter et al., 2007) and were conducted using the Greenhouse gases Observing SATellite (GOSAT) (Frankenberg, O'Dell, Guanter, & McDuffie, 2012; Guanter et al., 2012) and SCanning Imaging Absorption SpectroMeter for Atmospheric CHartographY (SCIAMACHY) (Joiner et al., 2012). More recently, the Global Ozone

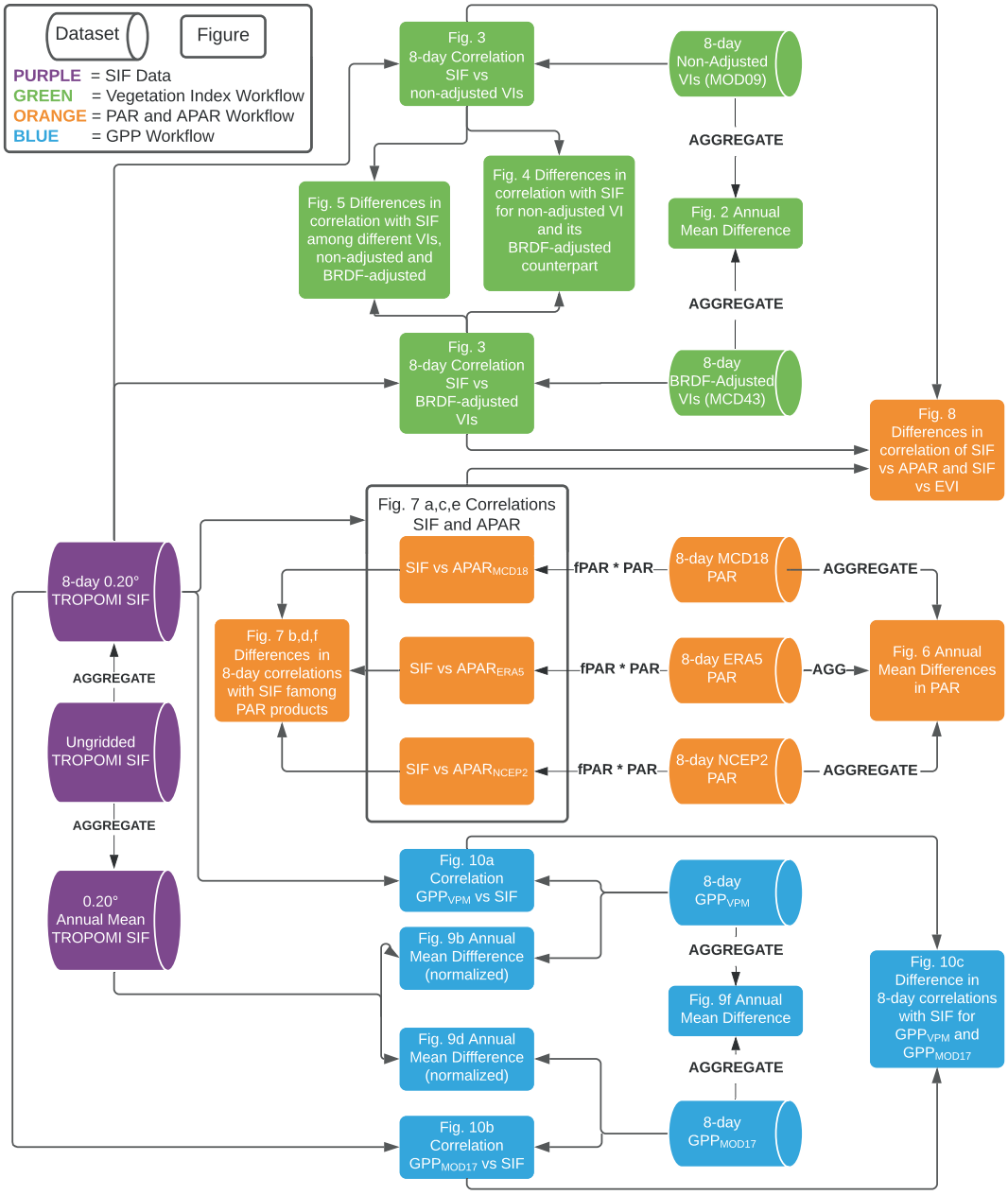

Figure 1. A diagram of the workflow undertaken in this study. Shown are the data sets (cylinders) we used and the figures (rectangles) we produced from those data sets. TROPOMI SIF data is in purple, and the workflows involving vegetation indices, photosynthetically active radiation (PAR) and absorbed photosynthetically active radiation (APAR), and gross primary production (GPP) are illustrated in green, orange, and blue, respectively.

Monitoring Experiment–2 (GOME-2) (Joiner et al., 2013) and Orbiting Carbon Observatory-2 (OCO-2) (Frankenberg et al., 2014) have been used to retrieve SIF. Many studies have studied the relationships between SIF and GPP (Porcar-Castell et al., 2014; Sun et al., 2018), developed SIF-GPP models for estimating GPP (Guan et al., 2015; Porcar-Castell et al., 2014), and used SIF data from GOME-2 and OCO-2 to evaluate GPP data products (Sun et al., 2017; Wagle et al., 2016; Y. Zhang et al., 2016).

Currently, the relationship between sun-sensor geometry and retrieved SIF is not fully understood, so a BRDF-like adjustment of spaceborne SIF data, from any platform, has not been conducted (Joiner et al., 2020; Köhler et al., 2018). Also, unlike surface reflectance data, SIF data is not strictly filtered for cloud cover as SIF is affected by cloud cover to a much smaller degree (Doughty et al., 2021; Guanter

et al., 2015; Köhler et al., 2018). It is also worth noting that SIF is emitted energy, not reflected energy, and thus a reflectance function is inherently inappropriate for emitted energy. Thus, a BRDF-like adjustment of the spaceborne SIF data, if it were shown to be appropriate and necessary, could only be applied to cloud-free observations (which would introduce clear sky bias) unless the BRDF adjustment could account for different fractions of cloud cover.

Nevertheless, we used two methods that partially account for the effect of sun-sensor geometry and reduces retrieval uncertainty. These two methods have been employed and discussed in greater detail in our previous publications (Doughty et al., 2019; Frankenberg et al., 2011; Köhler et al., 2018; Sun et al., 2018). First, we accounted for differences in the acquisition time and solar illumination geometry of the instantaneous retrieval of SIF by calculating daily average SIF. This calculation was done by multiplying the daily correction factor and instantaneous SIF as provided in the ungridded SIF data. Second, we calculated 8-day mean daily SIF at 0.20° spatial resolution to reduce retrieval uncertainty by n and account for differences in sensor viewing geometry. The rationale for using 8-day means to account for viewing geometry and the choice of 0.20° spatial resolution is as follows.

TROPOMI has a 16-day revisit cycle, meaning that the satellite's nadir track is slightly offset from the previous day and thus the angle between TROPOMI's sensor and any given point on Earth varies day-to-day. The viewing geometry over an 8-day period is comparable to the viewing geometry over the subsequent 8 days, as demonstrated in Figure S1. This figure is an ideal scenario, but what is important is not that the viewing angles of each 8-day span are identical but that the distribution of the viewing angles in each 8-day span are relatively uniform across the range of viewing angles. We have demonstrated these distributions for two gridcells in Figure S2.

Coincidentally, 8-day mean SIF affords us the opportunity to compare TROPOMI SIF to 8-day MODIS-based vegetation indices and GPP. Thus, we gridded TROPOMI SIF vector data into 8-day means starting on March 6, 2018, which corresponds to the temporal resolution of the 8-day MODIS-based products and is the earliest date for which we have TROPOMI data. Each SIF gridcell value was the area-weighted mean of all soundings within the gridcell over an 8-day period. We filtered the soundings with thresholds of 60° for viewing zenith angle, 0.8 for cloud fraction, 70° for solar zenith angles, and 120° for phase angles as described by Köhler et al. (2018). Finer resolution grids, such as 0.05°, severely impacts the SIF/GPP correlation, reduces the consistency of the 8-day data, and increases retrieval uncertainty (Figure S3). Conversely, coarser resolutions, such as 0.50°, have only minute differences with the 0.20° data.

2.2. Gross Primary Production Data Products

We compared the TROPOMI SIF data set with two MODIS-derived GPP data sets: GPP_{VPM} from the Vegetation Photosynthesis Model (VPM) (Y. Zhang et al., 2017) and GPP_{MOD17} from the MODIS MOD17A2H V006 product (Running & Zhao, 2015). Both GPP data sets have a spatial resolution of 500 m and a temporal resolution of 8 days. We aggregated both GPP data sets to 0.20° spatial resolution, which is consistent with TROPOMI SIF data set. Both GPP_{MOD17} and GPP_{VPM} are from light use efficiency (LUE) models.

$$GPP_{MOD17} = fPAR_{canopy} \times PAR \times \varepsilon_g \quad (6)$$

$$GPP_{VPM} = fPAR_{chl} \times PAR \times \varepsilon_g \quad (7)$$

where $fPAR_{canopy}$ is the fraction of PAR absorbed by the vegetation canopy and $fPAR_{chl}$ is the fraction of PAR absorbed by chlorophyll in the canopy. Note that $fPAR_{canopy}$ is substantially larger than $fPAR_{chl}$, as canopy is composed of both chlorophyll and non-photosynthetic vegetation (Q. Zhang et al., 2014, 2005), and the rationale for using $fPAR_{chl}$ instead of $fPAR_{canopy}$ is that $fPAR_{chl}$ captures information on only the photosynthetically active portion of the canopy (Xiao et al., 2004). The VPM model uses EVI calculated from MOD09A1 V006 surface reflectance (Vermote, 2015) to estimate $fPAR_{chl}$. The light use efficiency (ε_g) values in LUE models are calculated by downregulating maximum light use efficiency (often noted as ε_0) using environmental variables, such as temperature and water stress, and are different for each model. For detailed explanation of how LUE is calculated for the VPM and MODIS GPP data products, please see their respective data papers (Running et al., 2004; Y. Zhang et al., 2017).

2.3. MODIS Surface Reflectance Data and Vegetation Indices

We calculated the near-infrared reflectance of terrestrial vegetation (NIRv) (Badgley et al., 2017), Enhanced Vegetation Index (EVI) (Huete et al., 1997), and Normalized Difference Vegetation Index (NDVI) (Rouse et al., 1974) from two commonly used MODIS surface reflectance data products, MOD09A1 V006 (Vermote, 2015), and MCD43C4 V006 (C. Schaaf & Wang, 2015). The MOD09 data set is the standard MODIS surface reflectance product, and the MCD43 surface reflectance data set is adjusted for viewing geometry using the bidirectional reflectance distribution function (BRDF). For both surface reflectance products, we computed 8-day NIRv, EVI, and NDVI using the equations:

$$\mathrm{NIRv} = \frac{\mathrm{NIR} - \mathrm{RED}}{\mathrm{NIR} + \mathrm{RED}} \times \mathrm{NIR} \tag{8}$$

$$\mathrm{EVI} = 2.5 \times \frac{\mathrm{NIR} - \mathrm{RED}}{\mathrm{NIR} + 6 * \mathrm{RED} + 7.5 * \mathrm{BLUE} + 1} \tag{9}$$

$$\mathrm{NDVI} = \frac{\mathrm{NIR} - \mathrm{RED}}{\mathrm{NIR} + \mathrm{RED}} \tag{10}$$

The MOD09 EVI data that we used in this study was the same EVI data that was prepared for input into VPM. We derived MOD09 NIRv and NDVI using the same methods that were used to derive the MOD09 EVI data. More specifically, poor quality data were identified, data gaps were filled, and the data was smoothed using the Best Index Slope Extraction algorithm, linear interpolation, and the Savitzky-Golay filter as detailed by (Y. Zhang et al., 2017). The native spatial resolution of these MOD09 VIs is 500 m, and we aggregated these VIs to 0.20° spatial resolution.

The MCD43C4 data we used to calculate VIs is a daily product, which we aggregated temporally to 8-day means. This data set, which is provided in 0.05° spatial resolution, is produced using 16 days of Terra and Aqua MODIS data, and is weighted to the ninth day of the retrieval period (C. Schaaf & Wang, 2015). After calculating the VIs using the original MCD43C4 data, we aggregated the VIs to 0.20°. The methods used to derive the MCD43 data set are intended to remove the effects of viewing angle and directional reflectances, so the surface reflectance in this data set approximates what the reflectance would be if it were observed at nadir during the local solar noon (C. Schaaf & Wang, 2015).

2.4. Photosynthetically Active Radiation, fPAR, and APAR

For this study, we calculated 8-day mean PAR as a fraction (0.48) of the downward shortwave radiation at the surface estimated by three climate data sets: MODIS MCD18A2 (D. Wang, 2017), NCEP Reanalysis-2 (Kanamitsu et al., 2002), and ERA5: Fifth generation of ECMWF atmospheric reanalysis of the global climate (Copernicus Climate Change Service, 2017). These data sets were resampled or aggregated to 0.20° from their native spatial resolutions (5-km, ~1.9°, and 0.1°, respectively) and to 8-day means from their native temporal resolutions (6, 3, and 1-h, respectively). We calculated $\mathrm{APAR_{chl}}$ as $\mathrm{fPAR_{chl}} \times \mathrm{PAR}$ where $\mathrm{fPAR_{chl}}$ was a linear function of MOD09 EVI ($\mathrm{fPAR_{chl}} = (\mathrm{EVI} - 0.1) \times 1.25$) as detailed by Zhang et al. (2017).

3. Results

3.1. Differences Between Non-Adjusted NIRv, EVI, and NDVI and Their BRDF-Adjusted Counterparts and Their Correlations With TROPOMI SIF

There were very substantial latitudinal differences between non-adjusted and BRDF-adjusted vegetation indices that would affect estimates of $\mathrm{fPAR_{chl}}$ and $\mathrm{fPAR_{canopy}}$. Non-adjusted NIRv was moderately lower than BRDF-adjusted NIRv in the tropical and subtropical regions, and substantially higher than BRDF-adjusted NIRv at mid and high latitudes, except for far North Russia where non-adjusted NIRv was much lower than BRDF-adjusted NIRv (Figure 2a). Non-adjusted EVI was moderately lower in the tropics and substantially higher at mid and high latitudes compared to BRDF-adjusted EVI (Figure 2b). Non-adjusted NDVI was

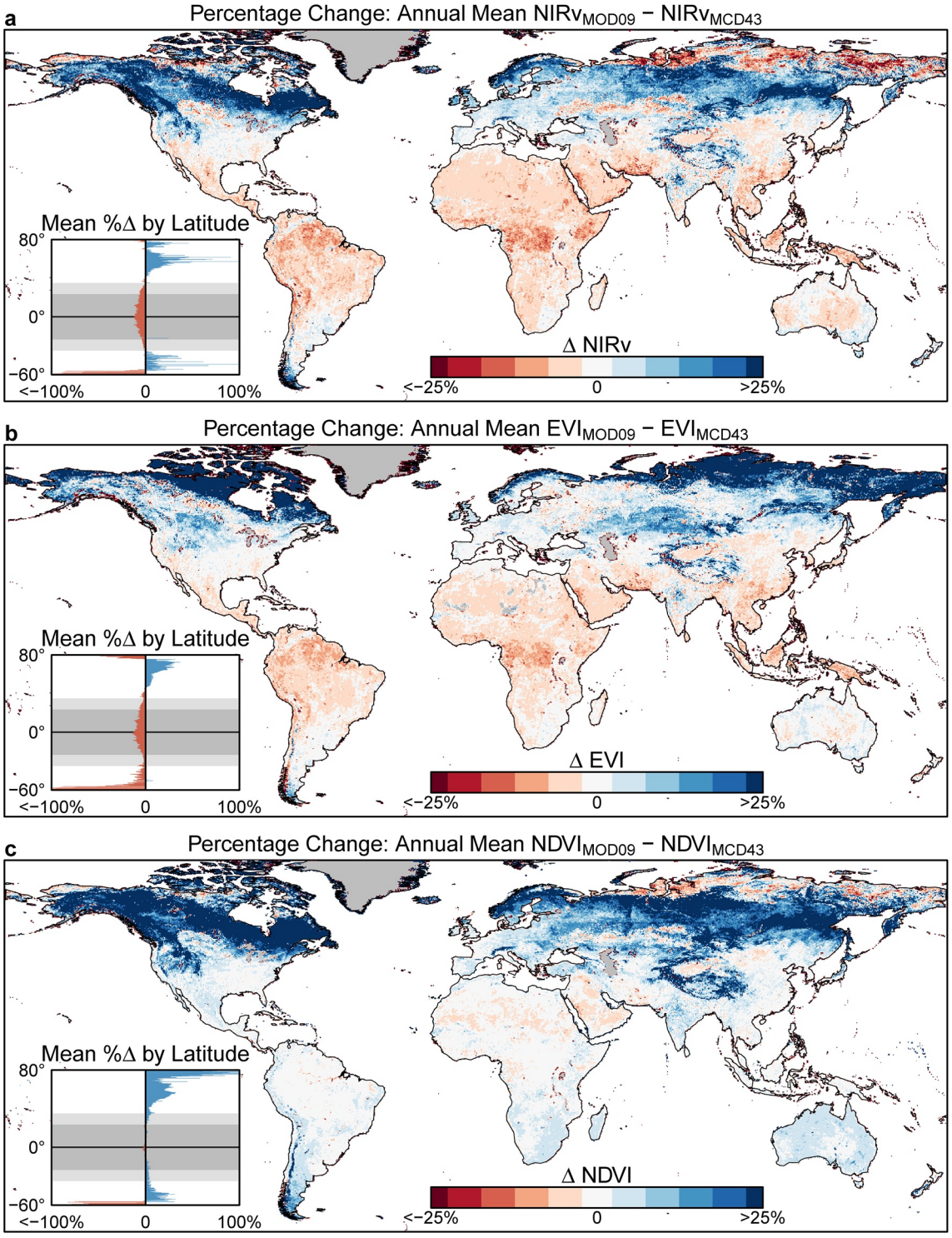

Figure 2. Percentage change between annual mean non-adjusted (MOD09) NIRv, EVI, and NDVI BRDF-adjusted (MCD43). Inset figures show mean percentage change by latitude; the dark shaded region represents the tropics (23.5°N to 23.5°S) and the light shaded region represents the subtropics (35°N and 35°S). Maps of the annual means for each vegetation index from each platform are depicted in Figure S4. Gray shaded terrain is no data.

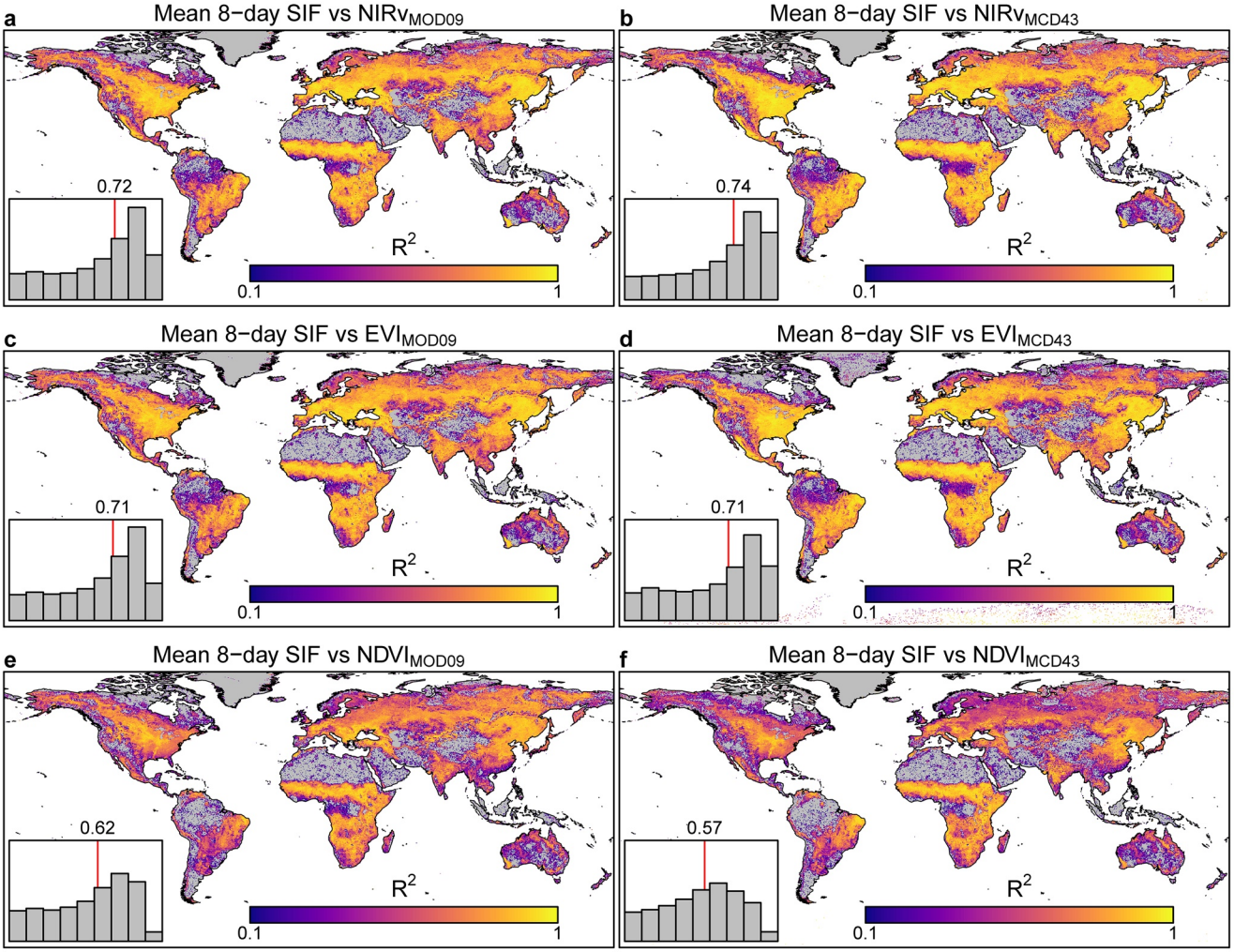

Figure 3. Temporal correlation between SIF and non-adjusted and BRDF-adjusted and NIRv, EVI, and NDVI in 2018 at 0.2° spatial resolution and 8-day temporal resolution. Temporal correlation between SIF and NIRv, EVI, and NDVI from non-adjusted MOD09 (a, c, and e) and BRDF-adjusted MCD43 (b, d, and f) surface reflectance data products at individual gridcells during the 2018 study period using 8-day data at 0.20° spatial resolution. Red lines in and values above the inset histograms indicate the median. Gray shaded terrain is no data or no significant correlation ($p > 0.05$).

substantially higher than BRDF-adjusted NDVI at high latitudes, except for far north Russia (Figure 2c). Despite these dramatic regional differences, we found at the global-scale that the mean percentage change between annual mean non-adjusted and BRDF-adjusted NIRv and EVI were rather negligible (−0.19% and −0.13%, respectively). For NDVI, the difference in the global annual mean was relatively large (6.94%). These geographic differences between non-adjusted and BRDF-adjusted vegetation indices highlights the need to consider the potential effect of the BRDF adjustment on GPP estimates at the pixel, regional, and global scales when these vegetation indices are used as proxies of fPAR.

In terms of the temporal consistency, TROPOMI SIF was strongly correlated with both non-adjusted and BRDF-adjusted NIRv, EVI, and NDVI throughout the year, except in the tropics where the correlation was often weak or not significant (Figure 3). The poor temporal correlation (R^2) in the tropical regions between 10°S and 10°N was most likely due to a weak seasonal amplitude in vegetation indices and SIF, fewer satellite observations, and more frequent cloud cover (Figures S5 and S6). However, we did notice that BRDF-adjusted NIRv and EVI was more likely to be significantly correlated with SIF in the Amazon and tropical Africa (Figures 3a–3d). We also found important differences in the temporal correlation between SIF and non-adjusted VIs and between SIF and their BRDF-adjusted counterparts. Non-adjusted NIRv had a weaker correlation with SIF than BRDF-adjusted NIRv across much of the globe (Figure 4a). The same

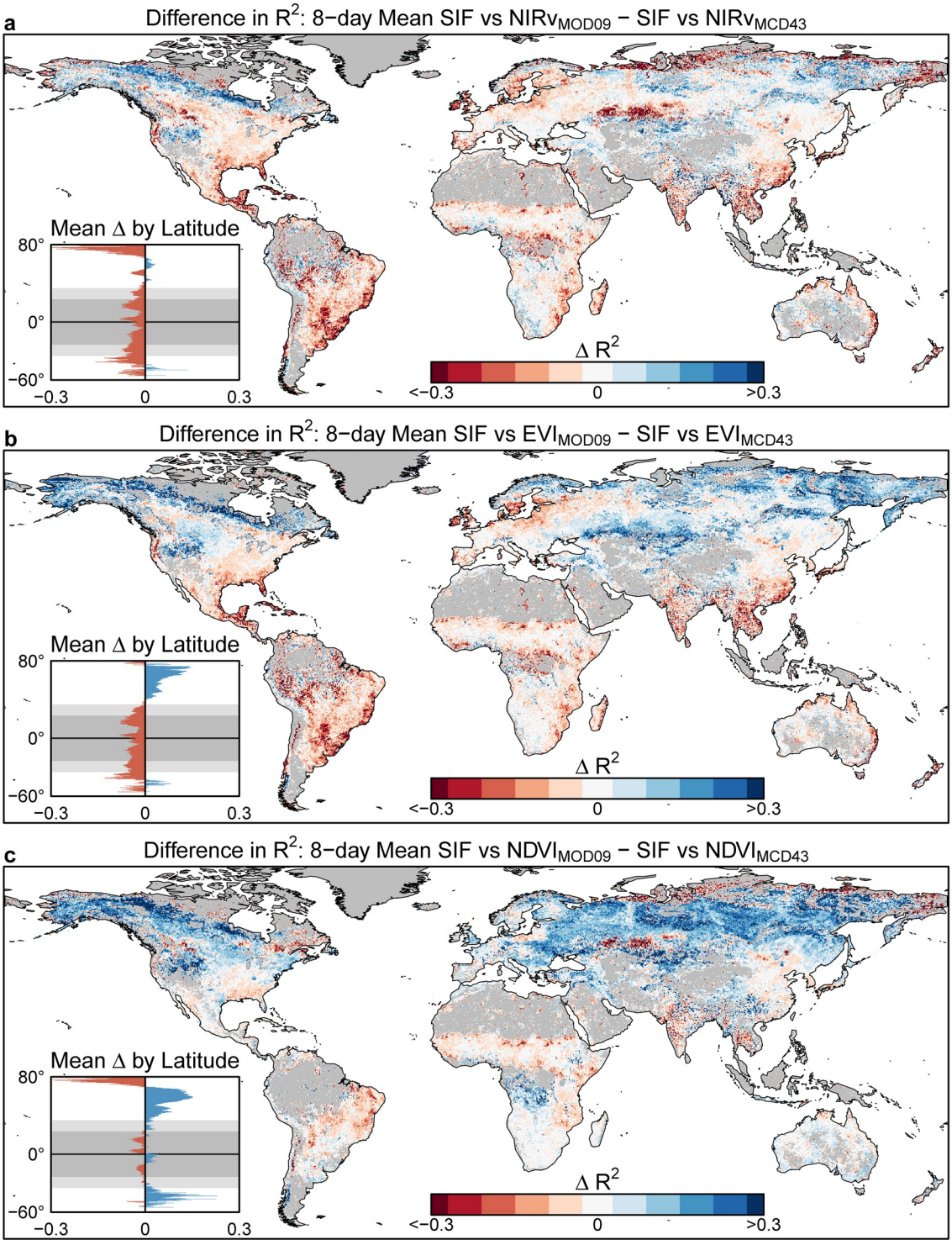

Figure 4. Differences in the temporal correlation (R^2) between SIF and non-adjusted and BRDF-adjusted and NIRv, EVI, and NDVI in 2018. Gray shaded terrain is no data or no significant correlation ($p > 0.05$). Inset figures show the mean difference in R^2 by latitude; the dark shaded region represents the tropics (23.5°N to 23.5°S) and the light shaded region represents the subtropics (35°N and 35°S).

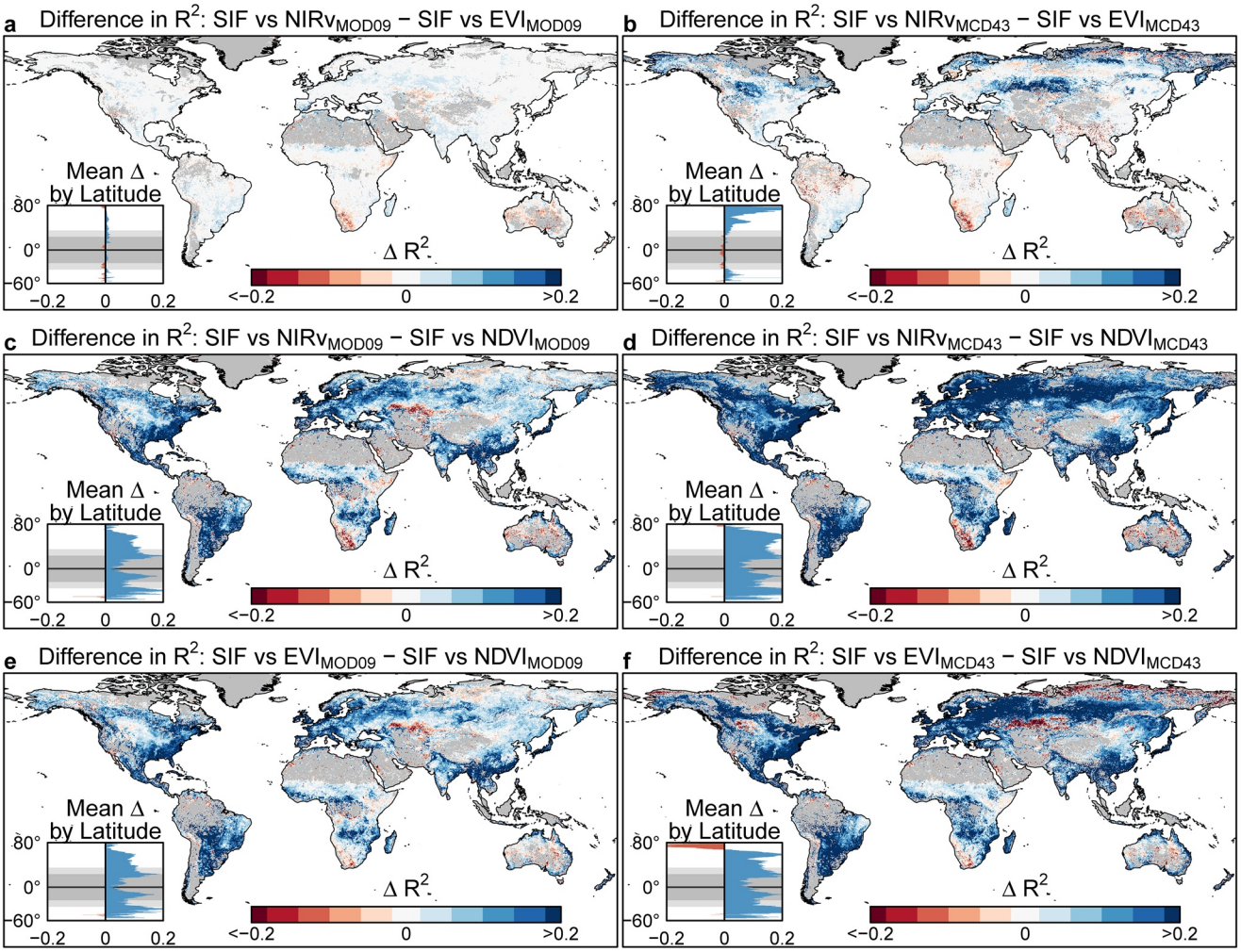

Figure 5. Differences in the temporal correlation (R^2) between 8-day TROPOMI SIF and non-adjusted and BRDF-adjusted NIRv, EVI, and NDVI. (a, c, and e) Differences in the temporal correlation (R^2) between TROPOMI SIF and non-adjusted (MOD09) NIRv, EVI, and NDVI. (b, d, and f) The same for TROPOMI SIF and BRDF-adjusted (MCD43) indices. These difference maps were computed using the R^2 maps in Figure 3. Gray shaded terrain is no data or no significant correlation ($p > 0.05$). Inset figures show the mean difference in R^2 by latitude; the dark shaded region represents the tropics (23.5°N to 23.5°S) and the light shaded region represents the subtropics (35°N and 35°S).

was true for non-adjusted EVI, except in the northern temperate zone where non-adjusted EVI tended to be better correlated with SIF (Figure 4b). Non-adjusted NDVI tended to have a stronger correlation with SIF than BRDF-adjusted NDVI, especially in the northern temperate zone.

3.2. Differences in the Correlations of Non-Adjusted and BRDF-Adjusted NIRv, EVI, and NDVI With TROPOMI SIF

To investigate which vegetation index was most temporally consistent with TROPOMI SIF for both BRDF-adjusted and non-adjusted vegetation indices, we computed the difference between their coefficients of determination (R^2) (Figure 5). The difference in the temporal correlation of non-adjusted NIRv and EVI with TROPOMI SIF was rather negligible (Figure 5a), with the most noticeable difference being that EVI was more consistent with TROPOMI SIF than NIRv in southwestern Africa and most of Australia. The correlation between TROPOMI SIF and BRDF-adjusted NIRv was substantially higher than for BRDF-adjusted EVI in portions of the northern temperate zone (Figure 5b). The temporal consistency between SIF and NDVI was much weaker than for NIRv and EVI for both BRDF-adjusted and non-adjusted surface reflectances (Figures 5c–5f). Interestingly, for both BRDF-adjusted and non-adjusted vegetation indices, NDVI

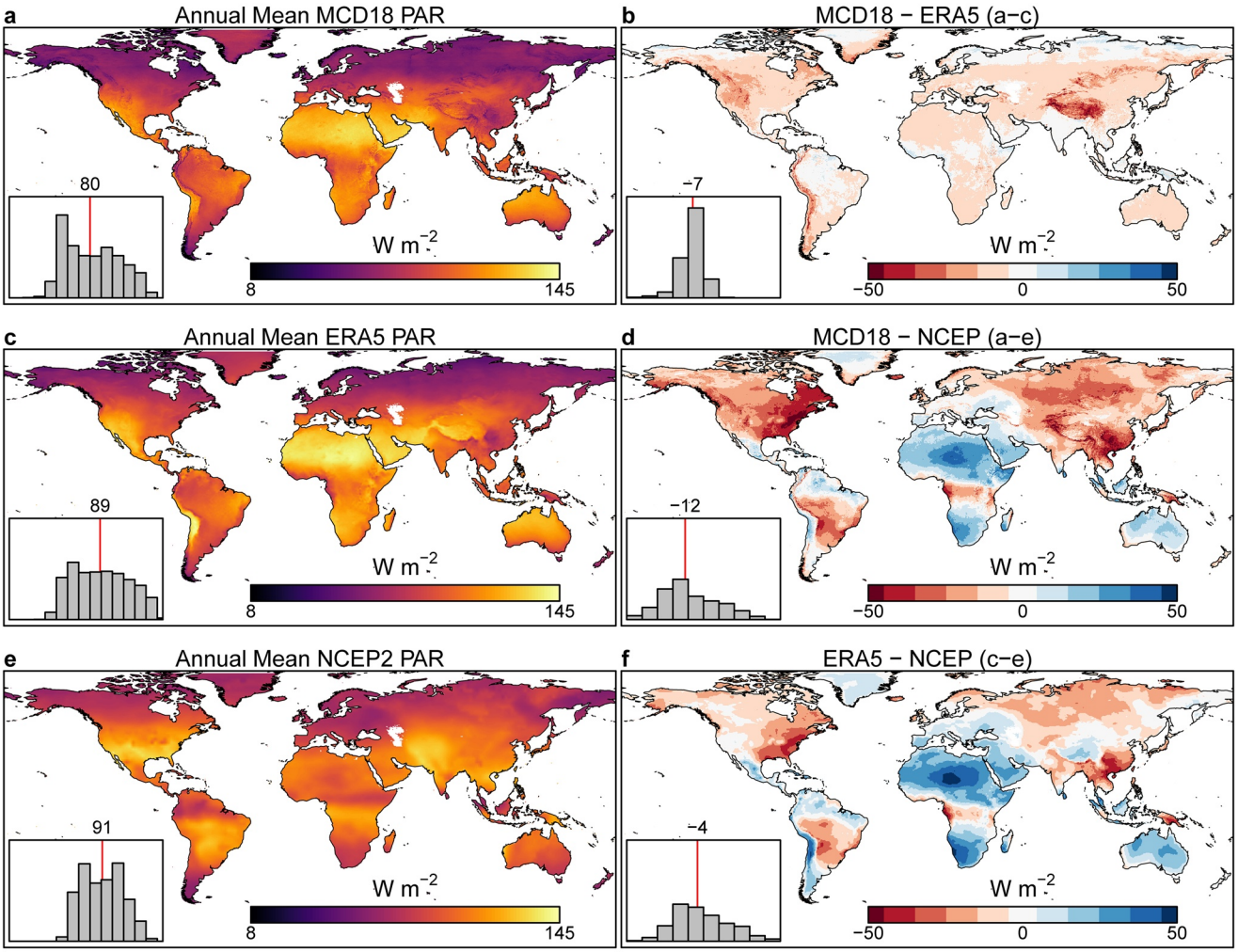

Figure 6. Annual mean PAR from NCEP-2, MCD18, and ERA5 and their differences. (a, c, and e) Annual mean PAR for the 2018 study period. (b, d, and f) Differences in annual mean PAR for the three data sets. Red lines in and values above the inset histograms indicate the median.

had a higher temporal consistency with SIF in southwest Africa and Australia's interior than either NIRv or EVI. The same was true in western Asia, except for BRDF-adjusted NIRv (Figure 5d).

3.3. Differences Between MCD18, ERA5, and NCEP2 PAR Products

The quality of PAR data affects the estimates of $APAR_{chl}$ and $APAR_{canopy}$ and may also affect the spatial and temporal consistency between TROPOMI SIF and $APAR_{chl}$ and $APAR_{canopy}$. When we compared the NCEP2, ERA5, and MCD18 PAR data, we found annual mean PAR (Figures 6a, 6c and 6e) to be very similar for MCD18 and ERA5 (Figure 6b), although MCD18 had lower estimates across most of the globe. However, there were stark differences between NCEP2 and the other two data sets (Figures 6d and 6f). The NCEP2 data had higher PAR estimates in North America, much of South America, tropical Africa, and Asia, and lower PAR estimates in Central America, northern South America, non-tropical Africa, much of southern Europe and the Middle East, and Australia.

3.4. Correlations of APAR With TROPOMI SIF and Their Differences

We used 8-day, non-adjusted EVI as a proxy of $fPAR_{chl}$, as is done in the VPM model, and the three PAR data sets to calculate three different estimates of $APAR_{chl}$ during the study period for temporal comparisons with

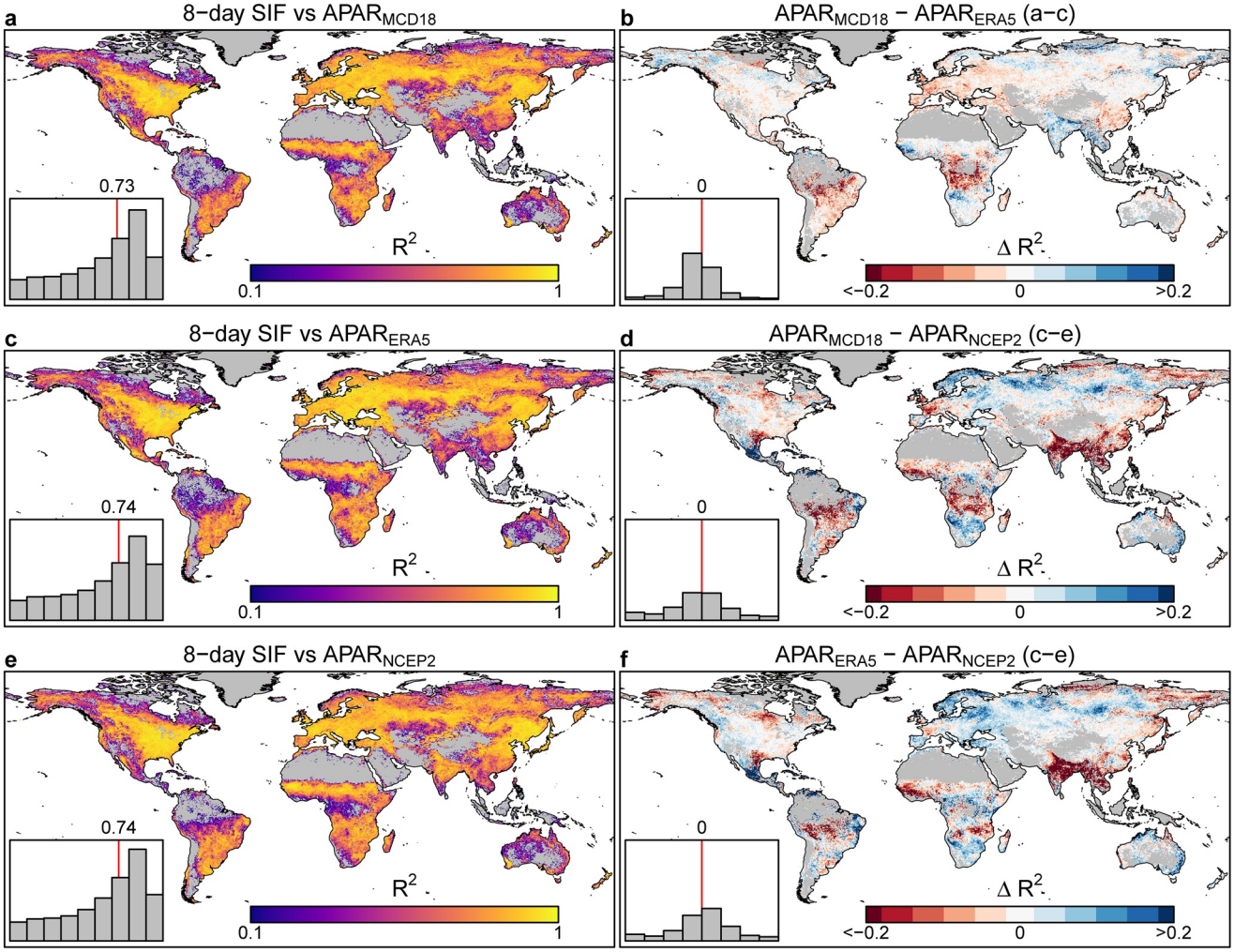

Figure 7. Temporal correlation between 8-day SIF and APAR for each of the three PAR data sets and their differences. (a, c, and e) Correlation between 8-day mean SIF and $APAR_{chl}$ calculated using PAR from NCEP2, MCD18, and ERA5 for the 2018 study period. (b, d, and f) Differences in the coefficients of determination (R^2) of SIF and $APAR_{chl}$ as calculated using the three PAR data sets. EVI_{MOD09} was used to estimate $APAR_{chl}$. Red lines in and values above the inset histograms indicate the median. Gray shaded terrain is no significant correlation ($p > 0.05$).

TROPOMI SIF. We found only minor differences among these three $APAR_{chl}$ data sets at the global-scale, with median global R^2 values between 0.73 and 0.74 (Figures 7a–7c). Geographically, there were relatively minor differences in the temporal correlation between SIF and $APAR_{chl}$ calculated from MCD18 and ERA5, with $APAR_{chl}$ from MCD18 having a weaker correlation with SIF in South America, tropical Africa, and Europe, but a stronger correlation in India, the Himalayan Region, and Indochina (Figure 7b). However, there were some stark differences in the temporal correlation between SIF and $APAR_{chl}$ calculated from NCEP2 and the other two PAR data sets (Figures 7d and 7f). Relative to $APAR_{chl}$ calculated using NCEP2 data, $APAR_{chl}$ calculated from MCD18 and ERA5 had much lower temporal correlations with SIF in northcentral and southcentral United States, tropical South America, subtropical Africa, India, the Himalayan Region, Indochina, southern and eastern China, but had stronger correlations in much of the boreal zone of Europe and Asia, southern Africa, and most of the Australian coast.

We further investigated whether there were differences in the temporal correlation of SIF with $APAR_{chl}$ and SIF with EVI, a proxy of $fPAR_{chl}$. Here, we again computed $APAR_{chl}$ from NCEP2, MCD18, and ERA5 PAR, but using both non-adjusted and BRDF-adjusted EVI as proxies of $fPAR_{chl}$. We found that the differences in the spatial distributions of the temporal correlation (R^2) between SIF/$APAR_{chl}$ and SIF/EVI to be very similar, regardless of the PAR product or EVI used to compute the difference (Figure 8). In each case, we

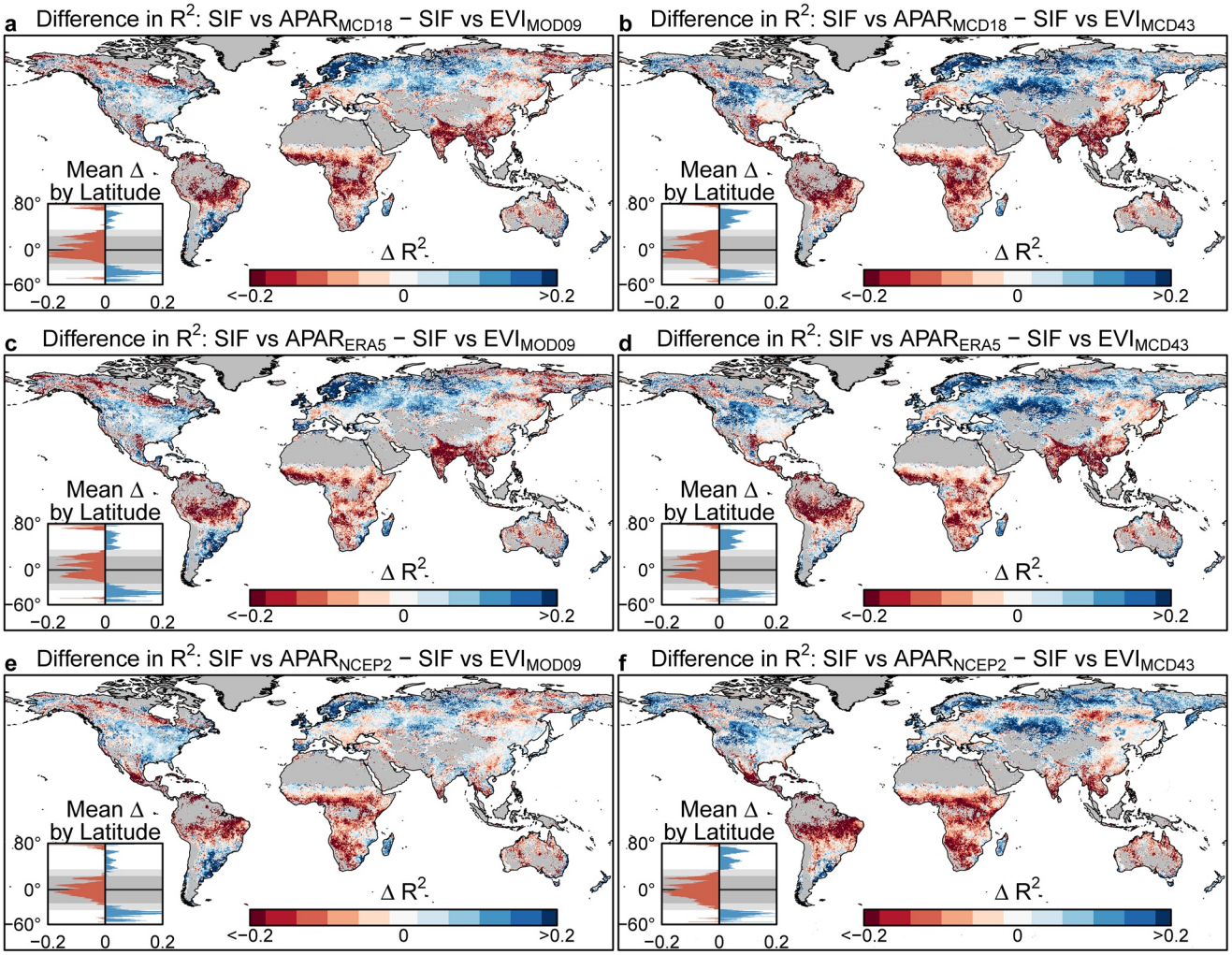

Figure 8. Differences in the temporal correlation of TROPOMI SIF with $APAR_{chl}$ calculated with NCEP2, MCD18, and ERA5 PAR data and non-adjusted and BRDF-adjusted EVI. (a, c, and e) Differences in the coefficients of determination (R^2) of SIF with $APAR_{chl}$ as computed from NCEP2, MCD18, and ERA PAR data and non-adjusted MOD09 EVI and (b, d, and f) BRDF-adjusted MCD43 EVI. The APAR values in each plot were calculated using the same EVI to which they are compared as a proxy of fPAR. Red lines in and values above the inset histograms indicate the median. Gray shaded terrain is no significant correlation ($p > 0.05$).

generally found $APAR_{chl}$ to be more consistent with SIF in the temperate zones and EVI to be more consistent with SIF in the tropics and subtropics. However, there were some regional differences that did not follow this general trend, such as in East Asia where SIF tended to be more strongly correlated with EVI than $APAR_{chl}$.

3.5. Differences and Correlations Between TROPOMI SIF, GPP_{VPM}, and GPP_{MOD17}

In terms of the spatial consistency between TROPOMI SIF, GPP_{VPM}, and GPP_{MOD17} in 2018, the spatial distributions of annual mean GPP_{VPM} and GPP_{MOD17} were highly consistent with annual mean SIF (Figures 9a, 9c and 9e; Figure S7). Relative to SIF, GPP_{VPM} was higher in the easternmost states of Brazil, Africa, and lower in Southeast Asia (Figure 9b), and GPP_{MOD17} was higher in Amazonia and was substantially lower in Sub-Saharan Africa and the cropland region of the Midwestern United States (Figure 9d). GPP_{MOD17} was lower than GPP_{VPM} in most of gridcells (Figure 9f).

In terms of temporal consistency at the gridcell level, 8-day GPP_{VPM} and SIF in 2018 were highly correlated (Figure 10a), except for the tropical regions where the seasonality of photosynthesis is relatively weak,

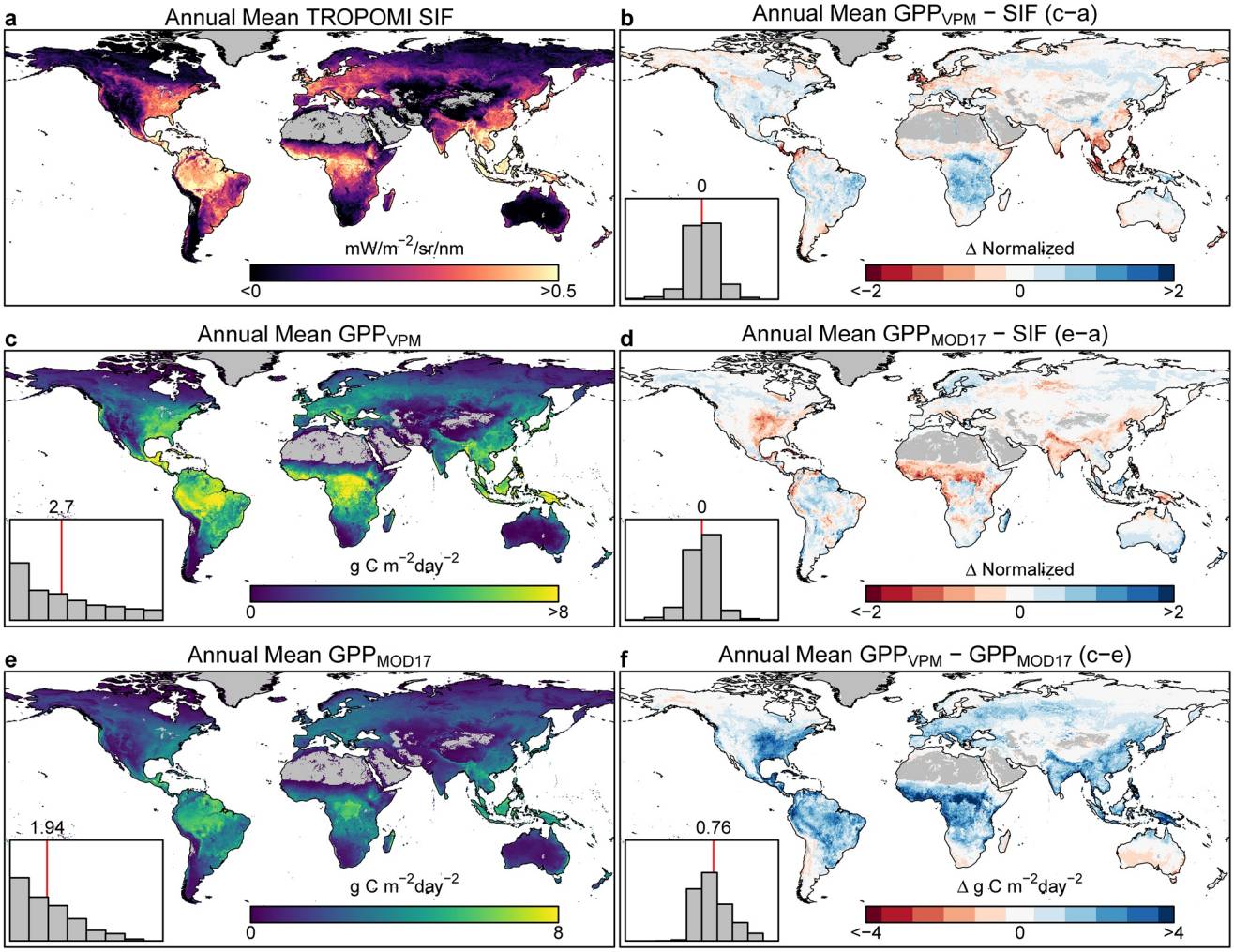

Figure 9. Mean annual TROPOMI SIF, GPP_{VPM}, and GPP_{MOD17} and their differences. (a, c, and e) Mean values for the 2018 study period. (b and d) Differences between normalized GPP and SIF. (f) Difference between GPP_{VPM} and GPP_{MOD17}. Red lines in and values above the inset histograms indicate the median. Gray shaded terrain is no data.

clouds are most persistent, and the number of good-quality satellite observations are low (Figures S5 and 6). Similarly, for GPP_{MOD17} there was a strong relationship with SIF at mid to high latitudes and weak or no relationships with SIF in the tropical regions (Figure 10b). However, there were also weak relationships in South America and in subtropical Africa. The difference between the 8-day consistency of GPP_{VPM} and GPP_{MOD17} with SIF was rather stark, with GPP_{VPM} having a stronger correlation with SIF across much of the globe, except in Sub-Saharan Africa (Figure 10c). Most notably, GPP_{VPM} had substantially stronger correlations with SIF in the South Central United States, South America, South Africa, India, and the provinces of South China. We also found that GPP_{VPM} had a significant relationship with SIF in ~8% more gridcells (20,813) than did GPP_{MOD17}.

4. Discussion

4.1. Potential Impacts of BRDF-Adjusted VIs on GPP Estimates

At the global-scale, we found mean annual non-adjusted NIRv and EVI to be slightly lower than BRDF-adjusted NIRv and EVI by 0.19% and 0.13%, respectively. However, non-adjusted NIRv and EVI had substantially higher values at high latitudes and substantially lower values in the tropics than BRDF-adjusted NIRv and EVI (Figure 2). These findings indicated that global annual mean GPP is likely to be higher when using

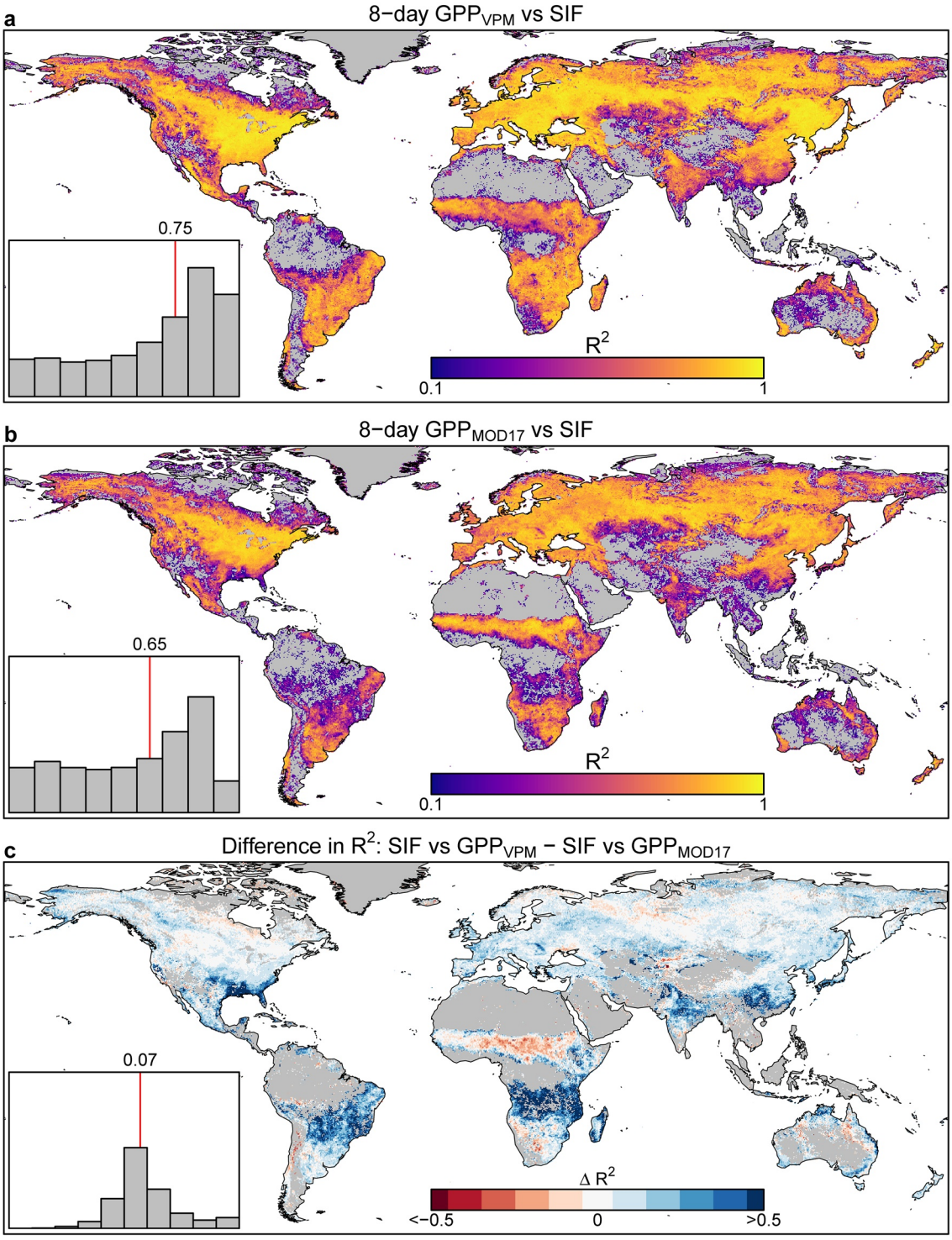

Figure 10. Temporal correlation between 8-day GPP_{VPM} and SIF, GPP_{MOD} and TROPOMI SIF, and their differences. (a and b) Temporal correlation between GPP and SIF at the gridcell level using 8-day data in 2018. (c) Difference between GPP_{VPM} temporal correlation with SIF and GPP_{MOD17} temporal correlation with SIF. Gray shaded terrain is no data or $p > 0.05$.

BRDF-adjusted NIRv or EVI as a proxy of fPAR, and that the use of BRDF-adjusted NIRv or EVI could result in substantially lower GPP at high latitudes and substantially higher GPP in the tropics relative to GPP estimates that use non-adjusted NIRv or EVI.

As for NDVI, the BRDF adjustment yielded substantially lower NDVI at the global-scale by nearly 7%, and there were substantially lower values at mid to high latitudes (Figure 2). Thus, the use of BRDF-adjusted NDVI as a proxy of fPAR to estimate GPP rather than non-adjusted NDVI would yield substantially lower estimates of GPP at mid and high latitudes, which would drive much lower estimates of global annual mean GPP at the global-scale.

BRDF-adjusted and NIRv and EVI were slightly more correlated with TROPOMI SIF at the global-scale than non-adjusted NIRv and EVI, with median R^2 higher by 0.02 and <0.01, respectively (Figure 3). However, BRDF-adjusted NIRv and EVI tended to be less correlated with SIF at mid to high latitude and more correlated with SIF in the Amazon and tropical Africa, as indicated by the white areas in northern South America and central Africa in Figures 3b and 3d. Thus, the use of BRDF-adjusted NIRv or EVI as a proxy of fPAR in modeling GPP would likely lead to stronger correlations between GPP and SIF in the tropics, but lower correlations at mid to high latitude. Globally, BRDF-adjusted NDVI had a lower correlation with SIF than non-adjusted NDVI, especially at mid to high latitude, but slightly higher correlations in most of South American and Africa.

Therefore, global mean annual GPP estimates and the correlation between SIF and GPP at the global-scale would likely not be substantially different when using non-adjusted NIRv or EVI as a proxy of fPAR. However, BRDF-adjusted NIRv and EVI would yield lower GPP estimates and lower correlations between SIF and GPP at high latitudes, and higher GPP estimates and higher correlations between SIF and GPP in the tropics relative to non-adjusted NIRv and EVI. These findings indicate that there is not a unidirectional benefit to using either BRDF-adjusted or non-adjusted NIRv and EVI as proxies of fPAR when estimating GPP, but rather there is a trade-off. For NDVI, there also appears to be a trade-off in that BRDF-adjusted NDVI has higher correlations with SIF in most of the tropics, but lower correlations at high latitude. However, the use of BRDF-adjusted NDVI would lead to substantially lower estimates of mean annual GPP, driven mostly by substantially lower estimates at mid to high latitudes.

4.2. Biophysical Performance of NIRv and EVI

Numerous vegetation indices have been proposed and calculated from the surface reflectance, and NDVI and EVI are two of the most used vegetation indices. NDVI is related to leaf area index and has been used to estimate $fPAR_{canopy}$ (Rouse et al., 1974; Running et al., 2004), but NDVI saturates when leaf area index is high (>3 m^2 m^{-2}) (Hinojo-Hinojo & Goulden, 2020). EVI was developed to account for the effect of the soil background and atmosphere on surface reflectance (Huete et al., 1997), and is used to estimate $fPAR_{chl}$ (Xiao et al., 2004). Over the last two decades, NDVI and EVI have been used as proxies of $fPAR_{canopy}$ and $fPAR_{chl}$, respectively, in LUE models to estimate GPP at the global-scale.

Recent studies reported that NIRv, which is a product of NDVI and NIR surface reflectance (Badgley et al., 2017; Dechant et al., 2019), addresses the NDVI-saturation issue over canopies with high LAI because NIR surface reflectance usually does not saturate. Badgley et al. (2017) reported a strong correlation between NIRv and GPP at eddy flux tower sites and also a stronger correlation between NIRv and GPP than between NIRv and GOME-2 SIF at 0.5° spatial resolution. These findings led the authors to advocate the use of NIRv for estimating global GPP. Similarly, we found a strong correlation between 8-day TROPOMI SIF and both BRDF-adjusted and non-adjusted NIRv at 0.2° spatial resolution. However, these correlations between TROPOMI SIF and non-adjusted NIRv were not substantially different than between TROPOMI SIF and non-adjusted EVI (Figure 5a). For BRDF-adjusted NIRv and EVI, NIRv was more highly correlated with SIF at high latitudes but EVI was more correlated with SIF in the tropics and subtropics (Figure 5b). Thus, we find that there is no clear advantage to using NIRv rather than EVI as a proxy of $fPAR_{chl}$.

Other studies have also found little difference in the ability of NIRv and EVI to track GPP or SIF. An analysis of GPP at six eddy covariance sites in Australia by Wang et al. (2019) found that OCO-2 SIF better captured the seasonal cycle (starting and ending dates) of GPP than NIRv because SIF values are not contaminated by background soil and different plant species contribute to the SIF signal additively. Likewise, Li et al. (2018)

found that OCO-2 SIF had a stronger relationship with GPP than NIRv using 64 eddy flux sites across the globe, and that NIRv and EVI performed very similarly. A study in the circumpolar region reported a closer agreement between SIF and GPP estimates than NIRv, EVI, and NDVI (Walther et al., 2018), and another study found NIRv, NDVI, and two-band EVI to perform relatively poorly in estimating the start and end of the growing season for tundra and grassland ecosystems (W. Yang et al., 2019).

Most recently, a study compared GPP estimates from 10 eddy towers across different vegetation types in California, United States, with BRDF-adjusted NIRv and EVI and found them to have nearly identical correlations with GPP both within and across sites (Hinojo-Hinojo & Goulden, 2020). These authors also conducted a global sensitivity analysis of NIRv and EVI to plant traits using the PROSAIL model and found that NIRv was slightly more sensitive to leaf chlorophyll content while EVI was slightly more sensitive to leaf area index. Both indices were nearly perfectly correlated linearly ($R^2 = 0.99$), and were nearly equally sensitive to leaf water content, leaf mass per area, leaf structure, mean leaf angle, and soil background.

As for NDVI, the propensity of NDVI to saturate where leaf area index is high caused NDVI to have relatively low correlations with SIF, particularly in the tropics. Our results, and the few studies that compare NIRv, EVI, SIF, and GPP, suggest that NIRv does not have a clear advantage over EVI in capturing the temporal dynamics if the vegetation canopy. However, because NIRv uses only the NIR and red portions of the spectrum, and EVI uses the blue, NIR, and red bands, NIRv is advantageous when the blue band is not available. NIRv is also thus more computationally inexpensive than EVI. It is also important to note that the use of the blue band in EVI can cause it to be sensitive to changes in canopy leaf carotenoid content, which are pigments that play a number of roles in photosynthesis (Frank & Cogdell, 1996). Nevertheless, further study is needed to understand how to incorporate NIRv and biophysically justify its use as a proxy of $fPAR_{chl}$ before it can be utilized to estimate GPP in the framework of LUE models.

4.3. GPP Estimates and PAR Input Data

$APAR_{chl}$ derived from the NCEP2, MCD18, and ERA5 PAR data are likely to yield different estimates of GPP at both spatial and temporal scales ($GPP = APAR_{chl} \times \varepsilon_g$). Our use of $fPAR_{chl}$ derived from non-adjusted EVI in calculating $APAR_{chl}$ for each data set ($APAR_{chl} = fPAR_{chl} \times PAR$) allowed us to investigate how the PAR data itself can yield differences in the correlation between $APAR_{chl}$ and TROPOMI SIF (Figure 7), and thus infer how these differences will affect the consistency between spaceborne GPP and SIF over space and time. Understanding what is driving the differences in the magnitude and timing of modeled GPP and spaceborne SIF is critical to improving the models and better understanding the role of photosynthesis in annual and seasonal fluxes of atmospheric carbon dioxide.

Compared to MCD18 and ERA5, NCEP2 has higher estimates of mean annual PAR in many of the most productive regions of the world, including North America, much of South America, tropical Africa, and nearly all of Asia (Figures 6d and 6f). This difference is important to note because the use of MCD18 or ERA5 PAR in estimating $APAR_{chl}$ would likely diminish the overall contribution of terrestrial photosynthesis to the global carbon flux. Regionally, NCEP2 PAR may yield lower annual GPP estimates in far northern South America, Central America, southern Africa, and Australia, where NCEP has relatively lower annual PAR estimates than MCD18 and ERA5. The use of PAR from MCD18 to derive $APAR_{chl}$ would likely yield lower annual GPP estimates than $APAR_{chl}$ derived from ERA5, as annual PAR from ERA5 is higher across the globe, particularly in the Tibetan Plateau and the Pacific Northwest of North America (Figure 6f).

The temporal consistency between SIF and modeled GPP is also strongly driven by which PAR data set is chosen. Most notably, $APAR_{chl}$ derived from NCEP2 PAR is much more temporally consistent with SIF in many of the most productive regions in the world, including India, the Himalayan region, Indochina, China, and much of North and South America (Figures 7d and 7f). Thus, use of NCEP2 PAR to derive $APAR_{chl}$ would yield GPP estimates that are more strongly correlated with SIF in these regions than if MCD18 or ERA5 were used. However, $APAR_{chl}$ derived from MCD18 and ERA5 tended to be more highly correlated with SIF in Central America, southern Africa, Australia, and the boreal region of Europe and Asia. Further research is needed to understand how the differences in the PAR data may affect the estimated timing of peak annual global photosynthesis, which has broader implications on understanding land-atmosphere carbon fluxes.

4.4. $APAR_{chl}$ and LUE Models

We expected SIF to be more highly correlated with $APAR_{chl}$ than EVI alone, because SIF is a function of both $fPAR_{chl}$ and the amount of incoming light energy (Magney, Frankenberg, et al., 2019; K. Yang et al., 2018). Instead, we found that SIF was generally more highly correlated with $APAR_{chl}$ at high to mid latitude and more highly correlated with EVI in the tropics (Figure 8), which helps explain why the correlation between SIF and GPP_{VPM} (Figure 10a) was likewise lower where EVI was better correlated with SIF than $APAR_{chl}$ (Figure 8a), as the VPM model is driven by $APAR_{chl}$. This finding suggests that these areas are likely light saturated, particularly in the tropics, in that changes in canopy chlorophyll drive changes in SIF rather than incoming sunlight at the top of the canopy. We observed this phenomenon in our previous study of the Amazon, where we found spaceborne SIF and eddy covariance tower GPP to mimic increased EVI despite decreased incoming PAR (Doughty et al., 2019).

However, the current models for the GPP_{VPM} and GPP_{MOD17} data products estimate daily GPP as a linear function of PAR ($GPP = fPAR \times PAR \times \varepsilon_g$), whereas the empirical response of GPP to light at the minute to hourly scale is logarithmic (Monteith, 1965; Smith, 1936). The response of SIF to light is also logarithmic at these coarse spatial and temporal scales (Magney, Barnes, & Yang, 2020; Porcar-Castell et al., 2014).

5. Conclusion

Here, we conducted a correlative analysis between TROPOMI SIF and (a) non-adjusted and BRDF-adjusted NIRv, EVI, and NDVI, (b) $APAR_{chl}$ as derived from non-adjusted and BRDF-adjusted EVI and PAR data from NCEP2, MODIS MCD43, and ERA5, and (c) GPP from two LUE models, VPM and MODIS GPP. We had five main findings. First, the correlation between SIF and non-adjusted NIRv and EVI were not substantially different, but there was a trade-off between BRDF-adjusted NIRv and EVI in that NIRv had higher correlations with SIF at mid to high latitude but lower correlations in the tropics. Second, BRDF-adjusted VIs had lower correlations with SIF at mid and high latitudes than non-adjusted VIs but had higher correlations in the tropics. Third, the choice of PAR data set could lead to substantial differences in GPP estimates at the global and regional scales, and to large differences in the correlation between SIF and modeled GPP. Fourth, SIF was more highly correlated with $APAR_{chl}$ than EVI at mid to high latitudes, but more highly correlated with EVI in the tropics. Finally, GPP_{VPM} had higher correlations with SIF than GPP_{MOD17}, except in sub-Saharan Africa.

Overall, we found that the choice of vegetation index as a proxy of fPAR and whether the index is BRDF-adjusted or not to come with trade-offs, in that no one option would greatly improve the correlation between modeled GPP and SIF at the global-scale. We found the same for the choice and PAR data set, as there are stark regional differences in the correlation between $APAR_{chl}$ computed from these data sets and SIF. However, substantial improvements in the correlation between modeled GPP and SIF are likely, particularly in the tropics, if LUE models were to model the response of GPP to PAR as being non-linear.

Data Availability Statement

The analysis and results were generated using publicly available data sets. TROPOMI SIF data is available at ftp://fluo.gps.caltech.edu/data/tropomi/, and aside from this FTP address there is no alternative method to access the data. The GPP_{VPM} data is available at https://doi.org/10.1594/PANGAEA.879560. MOD17A2H data is available at https://e4ftl01.cr.usgs.gov/MOLT/MOD17A2H.006/. MCD18A2 data is available at https://e4ftl01.cr.usgs.gov/MOTA/MCD18A2.006/. ERA5 data is available at https://cds.climate.copernicus.eu/. NCEP Reanalysis II data is available at https://psl.noaa.gov/data/gridded/data.ncep.reanalysis2.gaussian.html. MCD43C4 data is available at https://e4ftl01.cr.usgs.gov/MOTA/MCD43C4.006/. MOD09A1 data is available at https://e4ftl01.cr.usgs.gov/MOLT/MOD09A1.006/.

Acknowledgments
The authors are grateful to Vincent Humphrey for preparing the ERA5 data for analysis. This study was supported by research grants through the Geostationary Carbon Cycle Observatory (GeoCarb) Mission from NASA (GeoCarb Contract #80LARC17C0001), the US National Science Foundation: EPSCoR Program (IIA-1920946, IIA-1946093) and EEID program (1911955), the USDA National Institute of Food and Agriculture (2016-68002-24967), and the NASA OCO Science Team (80NSSC18K0895). Philipp Köhler and Christian Frankenberg were funded by the EARTH SCIENCE U.S. PARTICIPATING INVESTIGATOR (Grant: NNX15AH95G).

References

Badgley, G., Field, C. B., & Berry, J. A. (2017). Canopy near-infrared reflectance and terrestrial photosynthesis. *Science Advances*, *3*(3), e1602244. https://doi.org/10.1126/sciadv.1602244

Copernicus Climate Change Service. (2017). *ERA5: Fifth generation of ECMWF atmospheric reanalyses of the global climate*. Copernicus Climate Change Service Climate Data Store (CDS).

Dechant, B., Ryu, Y., Badgley, G., Zeng, Y., Berry, J. A., Zhang, Y., et al. (2019). Canopy structure explains the relationship between photosynthesis and sun-induced chlorophyll fluorescence in crops. *Remote Sensing of Environment*, *241*, 111733.

Doughty, R., Köhler, P., Frankenberg, C., Magney, T. S., Xiao, X., Qin, Y., et al. (2019). TROPOMI reveals dry-season increase of solar-induced chlorophyll fluorescence in the Amazon forest. *Proceedings of the National Academy of Sciences*, *116*(44), 22393–22398. https://doi.org/10.1073/pnas.1908157116

Doughty, R., Xiao, X., Qin, Y., Wu, X., Zhang, Y., & Moore, B., III (2021). Small anomalies in dry-season greenness and chlorophyll fluorescence for Amazon moist tropical forests during El Niño and La Niña. *Remote Sensing of Environment*, *253*, 112196. https://doi.org/10.1016/j.rse.2020.112196

Frank, H. A., & Cogdell, R. J. (1996). Carotenoids in photosynthesis. *Photochemistry and Photobiology*, *63*(3), 257–264. https://doi.org/10.1111/j.1751-1097.1996.tb03022.x

Frankenberg, C., Fisher, J. B., Worden, J., Badgley, G., Saatchi, S. S., Lee, J.-E., et al. (2011). New global observations of the terrestrial carbon cycle from GOSAT: Patterns of plant fluorescence with gross primary productivity. *Geophysical Research Letters*, *38*(17). https://doi.org/10.1029/2011gl048738

Frankenberg, C., O'Dell, C., Berry, J., Guanter, L., Joiner, J., Köhler, P., et al. (2014). Prospects for chlorophyll fluorescence remote sensing from the Orbiting Carbon Observatory-2. *Remote Sensing of Environment*, *147*, 1–12. https://doi.org/10.1016/j.rse.2014.02.007

Frankenberg, C., O'Dell, C., Guanter, L., & McDuffie, J. (2012). Remote sensing of near-infrared chlorophyll fluorescence from space in scattering atmospheres: Implications for its retrieval and interferences with atmospheric CO_2 retrievals. *Atmospheric Measurement Techniques*, *5*(8), 2081–2094. https://doi.org/10.5194/amt-5-2081-2012

Guan, K., Pan, M., Li, H., Wolf, A., Wu, J., Medvigy, D., et al. (2015). Photosynthetic seasonality of global tropical forests constrained by hydroclimate. *Nature Geoscience*, *8*(4), 284–289. https://doi.org/10.1038/ngeo2382

Guanter, L., Aben, I., Tol, P., Krijger, J. M., Hollstein, A., Köhler, P., et al. (2015). Potential of the TROPOspheric Monitoring Instrument (TROPOMI) onboard the Sentinel-5 Precursor for the monitoring of terrestrial chlorophyll fluorescence. *Atmospheric Measurement Techniques*, *8*(3), 1337–1352. https://doi.org/10.5194/amt-8-1337-2015

Guanter, L., Alonso, L., Gómez-Chova, L., Amorós-López, J., Vila, J., & Moreno, J. (2007). Estimation of solar-induced vegetation fluorescence from space measurements. *Geophysical Research Letters*, *34*(8). https://doi.org/10.1029/2007gl029289

Guanter, L., Frankenberg, C., Dudhia, A., Lewis, P. E., Gómez-Dans, J., Kuze, A., et al. (2012). Retrieval and global assessment of terrestrial chlorophyll fluorescence from GOSAT space measurements. *Remote Sensing of Environment*, *121*, 236–251. https://doi.org/10.1016/j.rse.2012.02.006

Hinojo-Hinojo, C., & Goulden, M. L. (2020). Plant traits help explain the tight relationship between vegetation indices and gross primary production. *Remote Sensing*, *12*(9), 1405. https://doi.org/10.3390/rs12091405

Huete, A. R., Didan, K., Miura, T., Rodriguez, E. P., Gao, X., & Ferreira, L. G. (2002). Overview of the radiometric and biophysical performance of the MODIS vegetation indices. *Remote Sensing of Environment*, *83*(1), 195–213. https://doi.org/10.1016/s0034-4257(02)00096-2

Huete, A. R., Liu, H. Q., Batchily, K. V., & van Leeuwen, W. J. D. (1997). A comparison of vegetation indices over a global set of TM images for EOS-MODIS. *Remote Sensing of Environment*, *59*(3), 440–451. https://doi.org/10.1016/s0034-4257(96)00112-5

Joiner, J., Guanter, L., Lindstrot, R., Voigt, M., Vasilkov, A. P., Middleton, E. M., et al. (2013). Global monitoring of terrestrial chlorophyll fluorescence from moderate-spectral-resolution near-infrared satellite measurements: Methodology, simulations, and application to GOME-2. *Atmospheric Measurement Techniques*, *6*(10), 2803–2823. https://doi.org/10.5194/amt-6-2803-2013

Joiner, J., Yoshida, Y., Köehler, P., Campbell, P., Frankenberg, C., van der Tol, C., et al. (2020). Systematic orbital geometry-dependent variations in satellite solar-induced fluorescence (SIF) retrievals. *Remote Sensing*, *12*(15), 2346. https://doi.org/10.3390/rs12152346

Joiner, J., Yoshida, Y., Vasilkov, A. P., & Middleton, E. M. (2011). First observations of global and seasonal terrestrial chlorophyll fluorescence from space. *Biogeosciences*, *8*(3), 637–651. https://doi.org/10.5194/bg-8-637-2011

Joiner, J., Yoshida, Y., Vasilkov, A. P., Middleton, E. M., Campbell, P. K. E., & Kuze, A. (2012). Filling-in of near-infrared solar lines by terrestrial fluorescence and other geophysical effects: Simulations and space-based observations from SCIAMACHY and GOSAT. *Atmospheric Measurement Techniques*, *5*(4), 809–829. https://doi.org/10.5194/amt-5-809-2012

Kanamitsu, M., Ebisuzaki, W., Woollen, J., Yang, S.-K., Hnilo, J. J., Fiorino, M., & Potter, G. L. (2002). NCEP-DOE AMIP-II Reanalysis (R-2). *Bulletin of the American Meteorological Society*, *83*(11), 1631–1643. https://doi.org/10.1175/bams-83-11-1631(2002)083<1631:nar>2.3.co;2

Köhler, P., Frankenberg, C., Magney, T. S., Guanter, L., Joiner, J., & Landgraf, J. (2018). Global retrievals of solar induced chlorophyll fluorescence with TROPOMI: First results and inter-sensor comparison to OCO-2. *Geophysical Research Letters*, *45*(19), 10456–10463. https://doi.org/10.1029/2018GL079031

Li, X., Xiao, J., He, B., Arain, M. A., Beringer, J., Desai, A. R., et al. (2018). Solar-induced chlorophyll fluorescence is strongly correlated with terrestrial photosynthesis for a wide variety of biomes: First global analysis based on OCO-2 and flux tower observations. *Global Change Biology*, *24*(9), 3990–4008. https://doi.org/10.1111/gcb.14297

Lin, X., Chen, B., Zhang, H., Wang, F., Chen, J., Guo, L., & Kong, Y. (2019). Effects of the temporal aggregation and meteorological conditions on the parameter robustness of OCO-2 SIF-based and LUE-based GPP models for croplands. *Remote Sensing*, *11*(11), 1328. https://doi.org/10.3390/rs11111328

Maeda, E. E., Heiskanen, J., Aragão, L. E., & Rinne, J. (2014). Can MODIS EVI monitor ecosystem productivity in the Amazon rainforest? *Geophysical Research Letters*, *41*(20), 7176–7183. https://doi.org/10.1002/2014gl061535

Magney, T. S., Barnes, M. L., & Yang, X. (2020). On the covariation of chlorophyll fluorescence and photosynthesis across scales. *Geophysical Research Letters*, *47*(23), e2020GL091098. https://doi.org/10.1029/2020gl091098

Magney, T. S., Bowling, D. R., Logan, B. A., Grossmann, K., Stutz, J., Blanken, P. D., et al. (2019a). Mechanistic evidence for tracking the seasonality of photosynthesis with solar-induced fluorescence. *Proceedings of the National Academy of Sciences*, *116*(24), 11640–11645. https://doi.org/10.1073/pnas.1900278116

Magney, T. S., Frankenberg, C., Köhler, P., North, G., Davis, T. S., Dold, C., et al. (2019b). Disentangling changes in the spectral shape of chlorophyll fluorescence: Implications for remote sensing of photosynthesis. *Journal of Geophysical Research: Biogeosciences*, *124*(6), 1491–1507. https://doi.org/10.1029/2019jg005029

Miao, G., Guan, K., Yang, X., Bernacchi, C. J., Berry, J. A., DeLucia, E. H., et al. (2018). Sun-induced chlorophyll fluorescence, photosynthesis, and light use efficiency of a soybean field from seasonally continuous measurements. *Journal of Geophysical Research: Biogeosciences*, *123*(2), 610–623. https://doi.org/10.1002/2017jg004180

Monteith, J. L. (1965). Light distribution and photosynthesis in field crops. *Annals of Botany*, *29*(1), 17–37. https://doi.org/10.1093/oxfordjournals.aob.a083934

Morton, D. C., Nagol, J., Carabajal, C. C., Rosette, J., Palace, M., Cook, B. D., et al. (2014). Amazon forests maintain consistent canopy structure and greenness during the dry season. *Nature*, *506*(7487), 221–224. https://doi.org/10.1038/nature13006

Pastorello, G., Trotta, C., Canfora, E., Chu, H., Christianson, D., Cheah, Y.-W., et al. (2020). The FLUXNET2015 dataset and the ONEFlux processing pipeline for eddy covariance data. *Scientific Data*, *7*(1), 1–27. https://doi.org/10.1038/s41597-020-0534-3

Porcar-Castell, A., Tyystjärvi, E., Atherton, J., Van der Tol, C., Flexas, J., Pfündel, E. E., et al. (2014). Linking chlorophyll a fluorescence to photosynthesis for remote sensing applications: Mechanisms and challenges. *Journal of Experimental Botany*, *65*(15), 4065–4095. https://doi.org/10.1093/jxb/eru191

Rouse, J. W., Haas, R. H., Schell, J. A., & Deering, D. W. (1974). Monitoring vegetation systems in the Great Plains with ERTS. *NASA Special Publication*, *351*, 309.

Running, S. W., Nemani, R. R., Heinsch, F. A., Zhao, M., Reeves, M., & Hashimoto, H. (2004). A continuous satellite-derived measure of global terrestrial primary production. *AIBS Bulletin*, *54*(6), 547–560. https://doi.org/10.1641/0006-3568(2004)054[0547:acsmog]2.0.co;2

Running, S. W., & Zhao, M. (2015). *MOD17A2H MODIS/Terra Gross Primary Productivity 8-Day L4 Global 500m SIN Grid V006*. NASA EOSDIS Land Processes DAAC. https://doi.org/10.5067/modis/mod17a2h.006

Saleska, S. R., Wu, J., Guan, K., Araujo, A. C., Huete, A. R., Nobre, A. D., & Restrepo-Coupe, N. (2016). Dry-season greening of Amazon forests. *Nature*, *531*(7594), E4–E5. https://doi.org/10.1038/nature16457

Schaaf, C., & Wang, Z. (2015). *MCD43A4 MODIS/Terra+ Aqua BRDF/Albedo Nadir BRDF Adjusted RefDaily L3 Global-500m V006*. NASA EOSDIS Land Processes DAAC.

Schaaf, C. B., Gao, F., Strahler, A. H., Lucht, W., Li, X., Tsang, T., et al. (2002). First operational BRDF, albedo nadir reflectance products from MODIS. *Remote Sensing of Environment*, *83*(1–2), 135–148. https://doi.org/10.1016/s0034-4257(02)00091-3

Smith, E. L. (1936). Photosynthesis in relation to light and carbon dioxide. *Proceedings of the National Academy of Sciences of the United States of America*, *22*(8), 504–511. https://doi.org/10.1073/pnas.22.8.504

Sun, Y., Frankenberg, C., Jung, M., Joiner, J., Guanter, L., Köhler, P., & Magney, T. (2018). Overview of Solar-Induced chlorophyll Fluorescence (SIF) from the Orbiting Carbon Observatory-2: Retrieval, cross-mission comparison, and global monitoring for GPP. *Remote Sensing of Environment*, *209*, 808–823. https://doi.org/10.1016/j.rse.2018.02.016

Sun, Y., Frankenberg, C., Wood, J. D., Schimel, D. S., Jung, M., Guanter, L., et al. (2017). OCO-2 advances photosynthesis observation from space via solar-induced chlorophyll fluorescence. *Science*, *358*(6360), eaam5747. https://doi.org/10.1126/science.aam5747

Turner, A. J., Köhler, P., Magney, T. S., Frankenberg, C., Fung, I., & Cohen, R. C. (2019). A double peak in the seasonality of California's photosynthesis as observed from space. *Biogeosciences*, *17*(2), 405–422.

Vermote, E. (2015). *MOD09A1 MODIS/Terra Surface Reflectance 8-Day L3 Global 500m SIN Grid V006*. NASA EOSDIS Land Processes DAAC. https://doi.org/10.5067/MODIS/MOD09A1.006

Wagle, P., Zhang, Y., Jin, C., & Xiao, X. (2016). Comparison of solar-induced chlorophyll fluorescence, light-use efficiency, and process-based GPP models in maize. *Ecological Applications*, *26*(4), 1211–1222. https://doi.org/10.1890/15-1434

Walther, S., Guanter, L., Heim, B., Jung, M., Duveiller, G., Wolanin, A., & Sachs, T. (2018). Assessing the dynamics of vegetation productivity in circumpolar regions with different satellite indicators of greenness and photosynthesis. *Biogeosciences*, *15*(20), 6221–6256. https://doi.org/10.5194/bg-15-6221-2018

Wang, C., Beringer, J., Hutley, L. B., Cleverly, J., Li, J., Liu, Q., & Sun, Y. (2019). Phenology dynamics of dryland ecosystems along the North Australian tropical transect revealed by satellite solar-induced chlorophyll fluorescence. *Geophysical Research Letters*, *46*(10), 5294–5302. https://doi.org/10.1029/2019gl082716

Wang, D. (2017).*MODIS/Terra+Aqua Photosynthetically Active Radiation Daily/3-Hour L3 Global 5km SIN Grid V006 [Data set]*.

Xiao, X., Hollinger, D., Aber, J., Goltz, M., Davidson, E. A., Zhang, Q., & Moore, B. (2004). Satellite-based modeling of gross primary production in an evergreen needleleaf forest. *Remote Sensing of Environment*, *89*(4), 519–534. https://doi.org/10.1016/j.rse.2003.11.008

Yang, K., Ryu, Y., Dechant, B., Berry, J. A., Hwang, Y., Jiang, C., et al. (2018). Sun-induced chlorophyll fluorescence is more strongly related to absorbed light than to photosynthesis at half-hourly resolution in a rice paddy. *Remote Sensing of Environment*, *216*, 658–673. https://doi.org/10.1016/j.rse.2018.07.008

Yang, P., & van der Tol, C. (2018). Linking canopy scattering of far-red sun-induced chlorophyll fluorescence with reflectance. *Remote Sensing of Environment*, *209*, 456–467. https://doi.org/10.1016/j.rse.2018.02.029

Yang, W., Kobayashi, H., Wang, C., Shen, M., Chen, J., Matsushita, B., et al. (2019). A semi-analytical snow-free vegetation index for improving estimation of plant phenology in tundra and grassland ecosystems. *Remote Sensing of Environment*, *228*, 31–44. https://doi.org/10.1016/j.rse.2019.03.028

Yang, X., Tang, J., Mustard, J. F., Lee, J.-E., Rossini, M., Joiner, J., et al. (2015). Solar-induced chlorophyll fluorescence that correlates with canopy photosynthesis on diurnal and seasonal scales in a temperate deciduous forest. *Geophysical Research Letters*, *42*(8), 2977–2987. https://doi.org/10.1002/2015gl063201

Yin, Y., Byrne, B., Liu, J., Wennberg, P. O., Davis, K. J., Magney, T., et al. (2020). Cropland carbon uptake delayed and reduced by 2019 Midwest floods. *AGU Advances*, *1*(1), e2019AV000140. https://doi.org/10.1029/2019av000140

Zhang, Q., Cheng, Y.-B., Lyapustin, A. I., Wang, Y., Gao, F., Suyker, A., et al. (2014). Estimation of crop gross primary production (GPP): FAPARchl versus MOD15A2 FPAR. *Remote Sensing of Environment*, *153*, 1–6. https://doi.org/10.1016/j.rse.2014.07.012

Zhang, Q., Xiao, X., Braswell, B., Linder, E., Baret, F., & Moore, B., III (2005). Estimating light absorption by chlorophyll, leaf and canopy in a deciduous broadleaf forest using MODIS data and a radiative transfer model. *Remote Sensing of Environment*, *99*(3), 357–371. https://doi.org/10.1016/j.rse.2005.09.009

Zhang, Y., Xiao, X., Jin, C., Dong, J., Zhou, S., Wagle, P., et al. (2016). Consistency between sun-induced chlorophyll fluorescence and gross primary production of vegetation in North America. *Remote Sensing of Environment*, *183*, 154–169. https://doi.org/10.1016/j.rse.2016.05.015

Zhang, Y., Xiao, X., Wu, X., Zhou, S., Zhang, G., Qin, Y., & Dong, J. (2017). A global moderate resolution dataset of gross primary production of vegetation for 2000–2016. *Scientific Data*, *4*, 170165. https://doi.org/10.1038/sdata.2017.165